Switchable Selectivity in Styrene Hydroformylation Using Single-Atom Rh Supported on g-C_3N_4 as Catalysts

Jie Pan[a], *Sergi Plana Ruiz*[b], *Mostafa Taoufik*[c], *Daniel Curulla-Ferré*[a,d*], *Josep M. Ricart*[a], *Cyril Godard*[a*]

[a] Departament de Química Física i Inorgànica, Universitat Rovira i Virgili, Tarragona 43007, Spain

[b] Servei de Recursos Científics i Tècnics, Universitat Rovira i Virgili, Tarragona 43007, Spain

[c] Univ. Lyon 1, CPE Lyon, CNRS UMR 5128, Laboratoire de Catalyse Polymérisation Procédés et Matériaux (CP2M), Université de Lyon, F-69616, France

[d] TotalEnergies OneTech Belgium, Feluy B7181, Belgium

ABSTRACT: A highly dispersed Rh catalyst supported on graphitic carbon nitride (Rh/g-C_3N_4) was used to investigate the hydroformylation of styrene. The results reveal that Rh/g-C_3N_4 exhibits high selectivity towards hydroformylation products; notably, no hydrogenated by-products were detected within the span of reaction conditions tested. An empirical model was developed to predict the selectivity to the branched (and linear) hydroformylation products using design of experiments, including three factors, temperature, partial pressure of carbon monoxide and partial pressure of hydrogen~~, was developed using design of experiments~~. The selectivity towards the branched aldehyde is favored at low temperatures and high pressures, the test at 100 bar confirmed the model prediction with an observed branched selectivity of 86.3%. Conversely, linear aldehydes are predominantly formed at high temperatures and low pressures, achieving the best selectivity to the linear aldehyde of 65.4% at 150 °C and 16 bar total pressure of CO/H_2 (1:1).

KEYWORDS: Styrene hydroformylation； Single atom catalysis； Design of experiments； Regioselectivity; Graphitic carbon nitride

Ha formatat: francès (Bèlgica)

Comentat [A1]: Compared to what value according to the model

Comentat [A2]: This is not what I would call «low pressure»

INTRODUCTION

With the development of nanotechnology, the dispersion of nanoscale catalysts has been further improved, by dispersing metals as single atoms on the carrier. In this context, g-C_3N_4 was extensively studied in recent years due to its simple synthesis methods, attractive electronic band structures and outstanding chemical properties.[1,2,3,4] g-C_3N_4 revealed as an outstanding support for single atom catalysts since the metal atoms are firmly trapped in the nitrogen-rich coordination sites.[5] Indeed, the lone pair of N atoms in g-C_3N_4 favors the coordination of transition metals, but also adjusts the electronic structures and performance, thus improve the catalyst properties.

The hydroformylation of alkenes (Scheme 1), which was originally discovered by Otto Roelen in 1938,[6] is one of the most important industrial applications of homogeneous catalysis.[7,8] From a synthetic point of view, the reaction is a one-carbon chain elongation reaction, caused by the addition of carbon monoxide and hydrogen across the π system of a C=C double bond.[9,10]

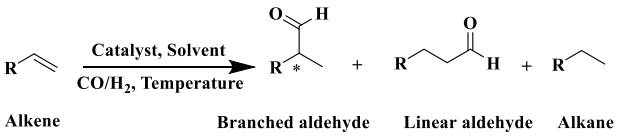

Scheme 1. Hydroformylation reaction of alkenes.

Recently, significant efforts have been made to develop heterogeneous catalysts for the hydroformylation of alkenes. And those based on isolated atoms or nanoparticles supported on inorganic oxides such as Al_2O_3[11], CeO_2[12] or CoO[13] have shown promising results in terms of activity. Indeed, highly dispersed and strongly anchored single atom catalysts (SACs) could present the advantages of both homogeneous and heterogeneous catalysts[14,15,16] and recently, several examples of SACs supported on nanomaterials were reported for the hydroformylation of alkenes.[11,17,18,19] However, the control of selectivity remains an issue for this type of catalysts.

ZnO nanowires supported Rh SACs (Rh_1/ZnO-nw) were reported to be competitive catalysts

for the styrene hydroformylation. In this study, pure SACs displayed high efficiency for styrene hydroformylation at 100 °C and 16 bar of CO/H_2 (1:1) with 99% selectivity to aldehydes. However, no regioselectivity was achieved as a linear/branched (l/b) ratio of 1 was obtained.[14] Wei and coworkers improved the linear selectivity using modified ZnO support anchored Rh SACs, a 90% conversion and 2.1 l/b selectivity were obtained at 100 °C and 40 bar CO/H_2 (1:1) for 4 h.[20] Li and colleagues modulated the selectivity to the linear aldehyde of the reaction via a coupling with low-temperature water-gas shift reaction catalyzed by Rh_1/CeO_2 SAC in water (3 ml) and dioxane (3 ml) mixed solvent at 120 °C for 12 h.[21] Recently, Axet and coworkers reported the preparation of Rh SACs on graphitic carbon nitride (g-C_3N_4) using $RhCl_3 \cdot 3H_2O$ as precursor followed by an activation at 550 °C. The catalysts were active in the hydroformylation reaction of styrene with high selectivity towards the aldehydes, ranging from 82% to 99%, and an l/b ratio of up to 1.6 at 90 °C and 20 bar of CO/H_2 (1:1).[22] In view of these results (Table S3), it can be concluded that the use of SACs in the hydroformylation of styrene favors the formation of the linear aldehyde.

In the hydroformylation of styrene, both linear and branched products are very important since the latter constitutes an important class of anti-inflammatory drugs while the linear product is used in the manufacture of detergents and plasticizers as well as intermediate in organic synthesis.[23,24,25] Therefore, it is of high interest to understand how reaction conditions influence the regioselectivity of this process.

Herein, g-C_3N_4 was selected as support to form Rh/ g-C_3N_4 SAC catalyst for further investigation on styrene hydroformylation as it proved resistant to high temperatures, oxygen, and in a variety of conventional solvents, including water, alcohols and toluene.[26] Aiming at determining the reaction conditions that favor the regioselectivity in styrene hydroformylation using such Rh/g-C_3N_4 SAC catalyst, a design of experiments (DOE) was used to investigate the relationship between conversion, selectivity and reaction conditions such as the temperature, the partial pressure of carbon monoxide and the partial pressure of hydrogen.[27,28]

EXPERIMENTAL

General materials

All chemicals and reagents were commercially available, with $Rh(acac)(CO)_2$ (CAS: 14874-82-9) storing in the desiccator, melamine (CAS: 108-78-1) in the ambient atmosphere. Solvents (toluene and hexane) were deoxygenated with argon before use, as detailed in the supporting information.

Synthesis of graphitic carbon nitride (g-C_3N_4)

Graphitic carbon nitride (g-C_3N_4) was synthesized by 99% melamine purchased from Sigma-Aldrich.[29,30] 20 g white powder, namely melamine was introduced into an alumina crucible (Scheme 2) with a lid and heated at 550 °C (with 5 /min ramp) in static air for 4 h. Subsequently, the yellow powder of g-C_3N_4 was grinded in a mortar after cooling down. 50% yield with 7.9 m^2/g Brunauer-Emmett-Teller (BET) surface was obtained. The surface was analyzed by diffuse reflectance infrared Fourier transform spectroscopy (DRIFT) and X-ray diffraction (XRD) (Figure S4), and showed similar featured when compared to previously reported data[31,32,33,34,35,36]

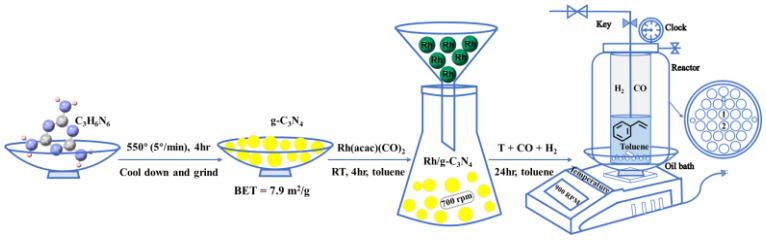

Scheme 2. Schematic diagram of catalysts synthesis and reaction conditions.

Synthesis of g-C_3N_4 supported Rh catalyst (Rh/g-C_3N_4)

The catalyst was prepared by an adsorption method (Scheme 2) aiming at a nominal loading of 0.01 wt%.[14,37] First, 2 g of g-C_3N_4 was dispersed in 150 ml deoxygenated toluene and stirred for

20 minutes at 700 rpm. At this point, 0.5 mg of $Rh(acac)(CO)_2$ dissolved in 5 mL toluene was added to the g-C_3N_4 suspension under stirring. Stirring was stopped after 3 hours, and the solution was aged for one more hour. Then, the catalyst was filtered and washed 3 times with hexane. Finally, the solid was dried under reduced pressure at room temperature and stored in a glovebox. Note that to minimize uncontrollable errors we synthesized this catalyst several times and mixed the batches together, to make sure all the tests were performed with the same catalyst.[14] Inductively Coupled Plasma Atomic Emission Spectrometry (ICP-OES) analysis was used to determine the Rh loading and a value of 0.007 ± 0.002 wt% was measured.

Characterization of Rh/g-C_3N_4

The sample was analyzed by scanning transmission electron microscopy (STEM) and Energy-dispersive X-ray spectroscopy (EDS). The EDS spectrum in (Figure 1(a)) evidenced the presence of C, N, O, and Rh species on one of the particles. High-angle annular dark-field scanning transmission electron microscopy (HAADF-STEM) provided information on the morphology of g-C_3N_4, and revealed layered structures with a particle diameter ranging from 200 to 300 nm (b_1 in Figure 1), but failed to detect Rh species (Figure 1(b)). The absence of Rh NPs suggested that the Rh species present at the support surface was single atoms or sub-nanoclusters. This result agrees with previous research by Axet and coworkers, who produced highly dispersed Rh single atoms on g-C_3N_4 with a rhodium metal loading of 0.1 wt%.[22]

Comentat [A3]: How did they conclude that they have single atoms? In any case, if they had single atoms at 0.1 %wt, surely we can imply that we have single atoms at 0.01 %wt.

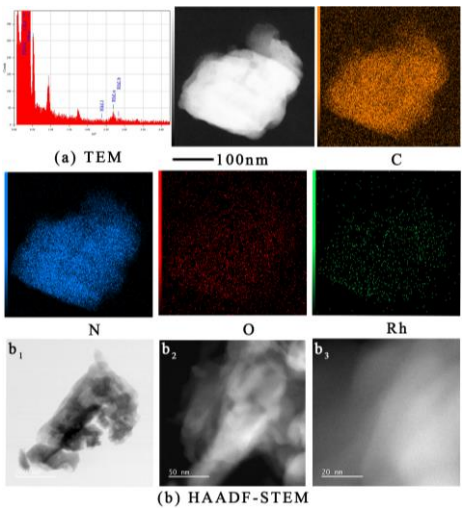

Figure 1. EDS spectrum and the respective elemental maps (a), Bright-Field and HAADF-STEM (b) images of 0.007 wt% Rh on g-C_3N_4.

In contrast, when DRIFTS upon CO adsorption (Figure S5) was used, weak bands could be observed at 2052 cm^{-1} and 2017 cm^{-1} that were assigned to symmetric and asymmetric stretches of the positively charged Rh $(CO)_2$ gem-dicarbonyl species and the peak at 1965 cm^{-1} associated with the linear-CO adsorption on Rh atoms. The absence of bridged-CO suggested that Rh was atomically dispersed on the g-C_3N_4 support. This result also matched the vibration frequencies obtained by density functional theory (DFT) calculations shown in Table S2. The calculated vibration frequencies from Axet et al. are also compared in Table S2 and consistent with our calculations.[22]

Based on DRIFTS and HAADF-STEM, it can be concluded that Rh atoms are highly dispersed on the surface of the g-C_3N_4 support, confirming the identity of these Rh species.

Comentat [A4]: I do not like this structure… I am not sure it is correct.

DESIGN AND RESULT

Exploratory data analysis

"Statistical thinking is making decisions based on data; a philosophy of learning and taking actions, based on the analysis, understanding and reduction of variation in a process".[38] In catalysis, we aim at developing a catalytic process that maximizes the yield towards a desired product, which is usually in competition with one or more other possible coproducts. Analyzing, understanding and reducing the variation in the process output is hence fundamental for optimizing the catalytic process. The output of a catalytic process depends on two types of variables: controllable and uncontrollable. By controllable, we mean that we can accurately set the value of such variable with high precision, whereas uncontrollable are usually other process or environmental variables for which we cannot set an accurate value, but that we can read or monitor with a certain level of precision. Usually, the controllable variables, also known as factors, are those that can be used to improve the catalytic process.

Several variables were identified to potentially influence the performance of the hydroformylation reaction in a batch reactor configuration: the metal used as catalyst, the support used to disperse the metal, the loading of the metal, the amount of catalyst used in the reaction, the nature of the solvent, the volume of the reactor, the volume of solvent, the reaction temperature, reaction time, partial pressure of carbon monoxide, partial pressure of hydrogen, presence of inert gases, agitation of the reaction mixture, aspect ratio of the reactor, etc. In the present study, we aim at studying the performance of highly dispersed Rh/g-C_3N_4 catalyst with a Rh nominal loading of 0.01 wt%; therefore, all the variables related to the catalyst are held constant. The reaction took place in a 24-position bath reactor equipped with 4 ml glass tubes, as pictures shown in Figure S6 (a). Hence, we limited ourselves to study the effect of the three process variables, namely, temperature, partial pressure of carbon monoxide and partial pressure of hydrogen. We could also present our analysis in terms of reaction temperature, total pressure and carbon monoxide to hydrogen molar ratio.

Temperature was allowed to change from a low value of 90 °C and up to a high value of 130 °C. Both carbon monoxide and hydrogen partial pressures were allowed to change between 10 bar and 20 bar, resulting in a total pressure spanning from 20 to 40 bar, and a CO-to-H_2 ratio from ½ to 2. These variables and their corresponding intervals of operation define a 3-dimensional space of possible experiments. Since there are no constraints when operating at any combination of reaction conditions within the defined experimental space, a full factorial design including a center point was used to build an experimental plan, with as few as 9 experiments (Table S4) to learn about the influence of the selected variables on the performance of the hydroformylation reaction. In order to estimate the experimental error each test was duplicated in the well of **1** and **2** marked in Scheme 2.

Comentat [A5]: By loading catalyst in positions 1 and 2 of the multitubular batch reactor.

The experimental results are shown in Table S5 and Figure 2. On the one hand, at the high catalyst/substrate ratio (0.016%), all conversions of styrene are > 75%, which is of importance for the study of selectivity. Selectivity to hydroformylation products is 100%, with no hydrogenation products observed for the entire experimental design space studied. Selectivity to the linear (SELL) and branched (SELB) hydroformylation are therefore anticorrelated. SELB ranges from as low as 40% at high temperature (130 °C) up to 60% at low temperature (90 °C). Figure 2 shows that higher SELB is systematically achieved at low temperatures (blue shadowed area). The span in the values of SELB at high temperature is narrow, ranging only from 40.5 to 44.1%. This seems to indicate that temperature is the most important variable in maximizing SELL, probably asymptotically reaching to a maximum value with increasing temperature and provided no parallel reaction channels are opened at higher temperatures; both carbon monoxide and hydrogen partial pressures have little effect on maximizing SELL. The mean value of SELB at low temperature is 53.5%, whereas at high temperature is only 41.7%, more than 10% points lower (Table S6).

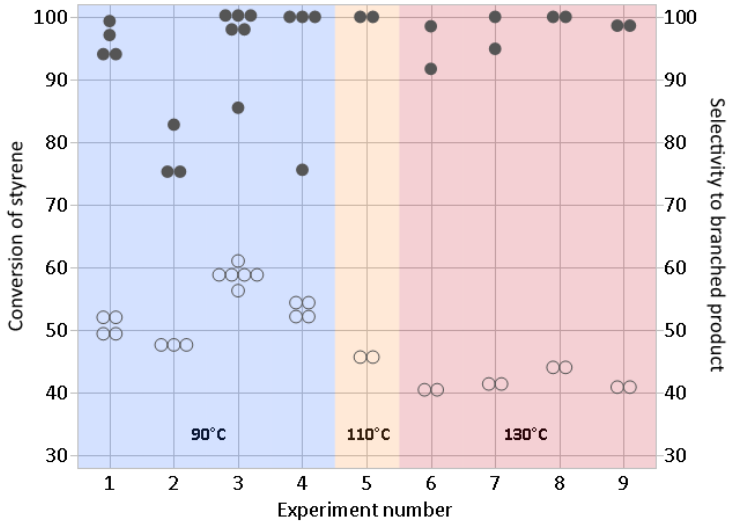

Figure 2. Conversion (filled discs) and selectivity towards the branched aldehyde (empty discs). The blue shadowed area highlights experiments done at 90 °C, the orange area at 110 °C and the red area at 130 °C.

The effect of pressure on SELB (Table S6) is somewhat more complex. Increasing total pressure leads to an increase in SELB, with a mean value for SELB of 44.8% at 20 bar up to 55.1% at 40 bar, an increase of 10.2% points. Similarly, increasing either the partial pressure of carbon monoxide or hydrogen led to an increase in SELB, however, the effect of each factor separately is less important than combined; from 46.3% at 10 bar of carbon monoxide to 52.4% at 20 bar (6.1% points increase), and from 47.0% at 10 bar of hydrogen to 51.8% at 20 bar (4.8% points increase). Expressed in terms of the ratio between the partial pressure of carbon monoxide and that of hydrogen, we observe an optimum value around a value of 1, with a SELB of 50.4%. If we decrease the ratio to 0.5, or increase it to 2.0, we observe an averaged SELB of approximately 48%.

A deep-dive analysis in the effect of the factors shows that the effect of temperature at high pressure (40 bar) on the SELB is twice as large as at low pressure (20 bar). The SELB at 90 °C increases from 47.7% at 20 bar total pressure to 58.7% at 40 bar (11% points increase), and from

40.5% at 130 °C and 20 bar, to 44.1% at 40 bar (3.6% points). The different increase in SELB with increasing temperature at different pressure reveals the presence of an interaction between these two factors (this can be seen graphically by the different slope as a function of pressure in Figure S7). Similarly, the effect of temperature at high partial pressure of carbon monoxide is larger than at low partial pressure, although it is not as pronounced; increasing the SELB from 49.4% at 90 °C and 10 bar partial pressure of carbon monoxide to 56.3% at 20 bar (7% points increase), and from 41.0% at 130 °C and 10 bar to 42.5% at 20 bar (1.5% points). The difference between high and low pressure is further decreased when considering the partial pressure of hydrogen; increasing from 50.6% at 90 °C at 10 bar partial pressure of hydrogen to 55.5% at 20 bar (4.9% points increase), and from 40.7% at 130 °C and 10 bar to 42.7% at 20 bar (2% points).

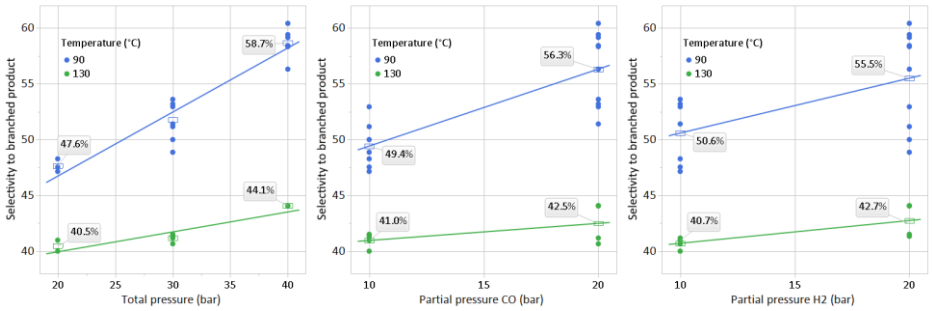

Figure 3. Effect of pressure on the SELB split by temperature.

The effect of pressure on the SELB is also influenced by the two-factor interaction between temperature and both partial and total pressure (Figure 3). We discussed above that the SELB increases with increasing total pressure from 44.8% at 20 bar total pressure up to 55.1% at 40 bar. However, this effect is more pronounced at low temperature (90 °C) where the SELB increases from 47.6% to 58.7% when increasing total pressure from 20 to 40 bar, whereas this increase is considerably less, from 40.5% to 44.1% at high temperature (130 °C). Similarly, we observe that

the SELB increases more with increasing partial pressure of carbon monoxide, from 49.4% to 56.3%, when temperature is low (90 °C), whereas at high temperature (130 °C), this increase is only from 41.0% to 42.5%. Finally, the SELB also increases more with increasing partial pressure of hydrogen, from 50.6% to 55.5%, at low temperature, and only from 40.7% to 42.7% at high temperature. We can observe again that the effect of increasing either the partial pressure of carbon monoxide or that of hydrogen is less significant than that of increasing total pressure.

In summary, SELB is favored at low temperatures and high pressures, with a carbon monoxide to hydrogen ratio close to one. On the contrary, SELL, which is anticorrelated with SELB as we did not observe any other products other than the hydroformylation products, is expected to be favored at high temperatures and low pressures.

Model for the selectivity

The design used in the present study enables us to build a linear model including the main (first-order) effects of the factors and two-factor interactions between them (Equation 1). The model also allows us to assess the degree of non-linearity of the data.

Equation 1

$$\hat{y}_{SELB} = b_0 + b_1 x_T + b_2 x_{PCO} + b_3 x_{PH2} + b_{12} x_T x_{PCO} + b_{13} x_T x_{PH2} + b_{23} x_{PCO} x_{PH2} + \varepsilon$$

Where $\hat{y}_{SELB}$ is the model prediction for the selectivity towards the branched hydroformylation product, which is a function of the three factors (reaction temperature, x_T, partial pressure of carbon monoxide, x_{PCO}, and partial pressure of hydrogen, x_{PH2}), ε represents the random error. Although such a model can be fitted and explain a large proportion of the variability in the data, it is physically incorrect, as one could obtain negative values for the selectivity or values above 1 (100%). Selectivity is, by its definition, a bound variable and therefore we need to transform the data so that its physical meaning is preserved in the model. One such transformation is the sigmoid transformation (Equation 2), that upon undoing the transformation enforces the response to be

bounded between 0 and 1, as required for modeling selectivity.

Equation 2

$$\hat{y}_{LSELB} = Log\left(\frac{\hat{y}_{SELB}}{1-\hat{y}_{SELB}}\right)$$

Where $\hat{y}_{SELB}$ is the predicted value for the SELB. The domain of the new variable, $\hat{y}_{LSELB}$, is from $-\infty$ to $+\infty$. If $\hat{y}_{LSELB}$ equals 0, then $\hat{y}_{SELB}$ equals 0.5 (50%), as $\hat{y}_{LSELB}$ becomes more positive $\hat{y}_{SELB}$ (asymptotically) approaches 1, and as $\hat{y}_{LSELB}$ becomes more negative, $\hat{y}_{SELB}$ approaches 0 (0%).

We can also transform the original factors, temperature, partial pressure of carbon monoxide and partial pressure of hydrogen, before fitting the model. One important such transformation is scaling (Equation 3). Scaled factors prevent from the model being biased due to different order of magnitude in the values of the various factors; this is not, however, the case in equation 1 in the present study, but we keep using scaled factors for the sake of best practice.

Equation 3

$$z_i = \frac{x_i - M_{x_i}}{\frac{R_{x_i}}{2}}$$

Where M_{x_i} is the midpoint of the domain of factor x_i used to build the model, and R_{x_i} is the range of the domain of factor x_i. The model that we will obtain is the resulting model from fitting the data to equation 4:

Equation 4

$$\hat{y}_{LSELB} = b_0 + b_1 z_T + b_2 z_{PCO} + b_3 z_{PH2} + b_{12} z_T z_{PCO} + b_{13} z_T z_{PH2} + b_{23} z_{PCO} z_{PH2} + \varepsilon$$

Or equivalently:

Equation 5

$$\hat{y}_{SELB} = \frac{1}{1 + exp(-(b_0 + b_1 z_T + b_2 z_{PCO} + b_3 z_{PH2} + b_{12} z_T z_{PCO} + b_{13} z_T z_{PH2} + b_{23} z_{PCO} z_{PH2}))} + \varepsilon$$

The model obtained from fitting the data to equation 4 is as follows:

Equation 6

$$\hat{y}_{LSELB} = -0.122 - 0.219 z_T + 0.082 z_{PCO} + 0.067 z_{PH2} - 0.051 z_T z_{PCO} - 0.025 z_T z_{PH2} + 0.027 z_{PCO} z_{PH2}$$

Equation 6 expressed in physical variables is included in the supporting material (Equation S1).

As shown in Table S7, all the model coefficients have a p-value well below 0.05 and they are therefore statistically significant. The model explains 96.7% of the variability in the data, upon correction for its complexity (number of terms in the model). The parity plot (Figure S8) for both the individual (left) and mean (right) values of the SELB shows that predictions are well within the confidence interval for a single prediction (light gray area).

The estimated experimental error of the linearized selectivity is calculated as the root mean square error (RMSE) of the model, which is 0.047. In order to estimate the experimental error of the untransformed selectivity, we need to calculate the error for each test used to build the model and averaged over all the tests; this results in an estimate error for the selectivity of 1.15% points. This value compares well with the actual experimental error that we can calculate from the pool of tests using Equation 7, which is 1.09%. This result shows that the model is a good approximation to predict the SELB of the reaction, within the design space defined for this study (Table S8). We can also observe that the largest error is obtained for the center point, thus showing there is a certain degree of non-linearity not accounted for in the model; however, this deviation is small and only of 1.24% points (Figure S9).

Equation 7

$$\sigma_E^2 = \frac{\sum_i \omega_i \sigma_i^2}{\sum_i \omega_i}$$

deviation for test i, and ω_i are the degrees of freedom (number of repetitions) of test i.

A final validation check of the model is the assessment of the behavior for the residuals, which should be normal, for a model properly representing the data. Figure S10 displays the cumulative distribution function (CDF) plot of the data and the corresponding normal CDF, showing a good match between the two curves, which allows us to conclude that the errors are distributed normally.

The parity plots (Figure S8) also show that temperature is the main factor explaining the different selectivity; this conclusion can also be drawn from the analysis of the coefficients, as (scaled) temperature has the largest absolute value coefficient (-0.219), followed up by the effect of partial pressure of carbon monoxide (0.082) and that of hydrogen (0.067). The factor-effect coefficients indicate that when we increase the scaled temperature (z_T) in one unit, the linearised selectiviy to the branched hydroformylation product decreases in 0.219 units, or in other words, when we increase the temperature in 20 °C, SELB decreases in 5.4% points or 0.27% points/°C. Similarly, when we increase the scaled partial pressure of carbon monoxide by one unit (5 bar), we increase the linearized SELB by 0.082 units or 2% points (0.1% points/bar CO), and if we increase the scaled partial pressure of hydrogen by one unit (5 bar), we increase the linearized SELB by 0.067 units or 1.6% points (0.8% points/bar H_2).

The model also includes three two-factor interactions; the interaction between temperature and partial pressure of carbon monoxide (-0.51), between temperature and partial pressure of hydrogen (-0.025) and between partial pressure of carbon monoxide and that of hydrogen (0.027). This means that the effect of increasing temperature depends on the values set for the pressure of carbon monoxide and hydrogen; hence, increasing temperature by 20 °C at low partial pressure of carbon monoxide (10 bar) decreases SELB in 4.1% points (1.3% points less than the 5.4% points pure

effect of temperature), whereas at high partial pressure of carbon monoxide (20 bar), SELB is decreased in 6.7% points (1.3% points more). This antagonistic interaction between temperature and partial pressure of carbon monoxide (and hydrogen) implies that we can maximize the SELB working at low temperature and high partial pressure of both carbon monoxide and hydrogen, or the SELL working at high temperatures and low partial pressure of both carbon monoxide and hydrogen.

Optimizing SELB and SELL

From the previous analysis of the data and of the model obtained (Equation 6), we need to decrease the temperature and increase both the partial pressure of carbon monoxide and hydrogen in order to maximize the selectivity towards the branched hydroformylation product. Setting 90 °C as the lowest temperature to run the reaction, Equation 6 can be reduced to:

Equation 8

$$\hat{y}_{LSELB} = 0.097 + 0.133z_{PCO} + 0.092z_{PH2} + 0.027z_{PCO}z_{PH2}$$

Equation 8 expressed in physical variables is included in Equation S2.

The contour plot (Figure 4) resulting from the application of Equation 8 in an extended range of partial pressure from 10 to 40 bar shows that in order to get a high selectivity towards the branched product, one needs to work at high pressure (i.e. 80 bar) and with a carbon monoxide to hydrogen ratio close to 1. Equation 8 predicts a SELB between 80.1% and 91.6% at 90 °C and 40 bar partial pressure of carbon monoxide and 40 bar partial pressure of hydrogen. The large length of the confidence interval (11.5% points) is due to the fact that we are extrapolating far from the design region in which the model was built.

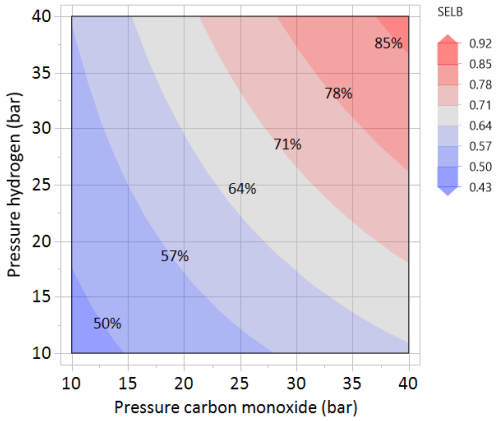

Figure 4. Contour plot of the SELB at 90 °C as a function of the partial pressures of carbon monoxide and hydrogen.

We therefore proceeded to perform a series of new experiments at higher pressure to confirm the predictions of the model (Table 1). All the new experiments were carried out at 90 °C varying the partial pressure of carbon monoxide and hydrogen in a range between 10 and 50 bar. We observe that the model predicts fairly well the experimental results (Table S9, Figure S11 and Figure 5); although for some experiments, the experimental selectivity observed falls outside the confidence interval of the prediction for an individual measurement, the discrepancy between the experimental and predicted values is small considering that the new experiments were done far from the design region used to build the model. The new experiment at 100 bar and a carbon monoxide to hydrogen ratio of 1 (#14) yield a SELB of 86.3%, whereas the predicted confidence interval for an individual measurement was between 88.2 and 98.1%. The second-best result obtained in the new experimental phase was at 50 bar and also a ratio of 1 (#11), which yielded a selectivity of 63.9%, well within the predicted confidence interval of 62.6 and 68.7%. All the other new experiments at 50 bar (#10, #12, #13), where the effect of the carbon monoxide to hydrogen ratio was explored varying it from ¼ to 4, performed worse than test #11 at a ratio of 1, hence

confirming the validity of the model in Equation 6 and the requirement to work with a carbon monoxide to hydrogen ratio of 1 to maximize the SELB.

Table 1 New experimental phase to optimize the SELB (tests 10-14) and to the linear product (tests 15-16).

Test	Temperature (°C)	CO pressure (bar)	H_2 pressure (bar)	Total pressure (bar)	H_2/CO ratio	Pred SELB
10	90	10	40	50	0.25	52.3 - 61.8%
11	90	25	25	50	1.00	62.6 – 68.7%
12	90	35	15	50	2.33	62.0 – 68.2%
13	90	40	10	50	4.00	58.4 – 67.4%
14	90	50	50	100	1.00	88.2 - 98.1%
15	140	8	8	16	1.00	32.7 – 41.0%
16	150	5	5	10	1.00	29.6 – 39.6%

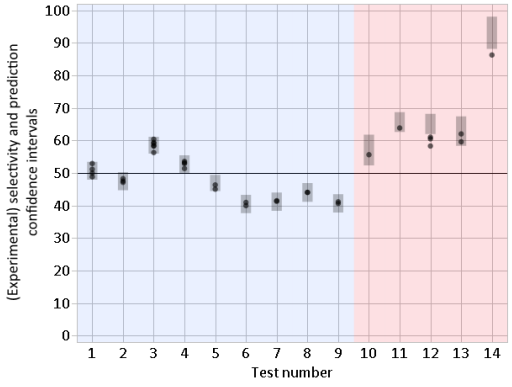

Figure 5. Experimental SELB (dots) and confidence intervals of the predictions using Equation 6. Blue shadowed area corresponds to the tests used to generate the model. Red shadowed area corresponds to the new experiments at higher pressures.

Using the new data to update the model, we produced a new model for predicting selectivity towards the branched hydroformylation product (Equation 9), which is very similar to Equation 6, but where the interaction between temperature and the partial pressure of hydrogen has been removed from the model. We can also observe that the importance of the effect of the partial pressure of hydrogen is similar to that of carbon monoxide, and that the effect of the interaction between the partial pressure of carbon monoxide and that of hydrogen is now more important than the interaction between temperature and the partial pressure of carbon monoxide.

Equation 9

$$\hat{y}_{LSELB} = 0.388 - 0.313z_T + 0.405z_{PCO} + 0.428z_{PH2} - 0.126z_T z_{PCO} + 0.205z_{PCO}z_{PH2}$$

The new model explains 97.4% of the variability in the data, upon correction for its complexity (number of terms in the model). The parity plots (Figure S12) for both the individual (left) and mean (right) values of the SELB show that predictions are well within the confidence intervals. The experimental error, including the new experiments, is 1.11%, whereas the estimated experimental error is the same as previously and equals 1.09%. The new model in equation 9 describes well the complete data set (tests 1-14). The center point of the first experimental phase, which was used to detect non-linearity in the first model, is not the one with largest deviation when using the second model (Figure S13); this could be interpreted as that the new model (Equation 9) does not show any significant non-linear deviation.

Finally, we wanted to maximize the SELL. Since we obtained 100% selectivity to hydroformylation products in all the experiments performed, the SELL and SELB are perfectly anticorrelated, and therefore, maximizing SELL is the same as minimizing SELB. Using equation 9 to model the SELB, we need to work at high temperatures and at low pressures to favor the production of the linear product; yet, it is important to note that the interaction effect between the partial pressure of carbon monoxide and that of hydrogen, which favors the production of the

branched product as both partial pressures increase or decrease, and the interaction between temperature and the partial pressure of carbon monoxide, which tends to reduce the effect of the partial pressure, limit the extent to which one could decrease both partial pressures simultaneously while increasing the temperature.

Another limitation facet when willing to maximize the linear product is that pressure and temperature cannot be reduced and increased independently, as this could favor the evaporation of the solvent and substrate. With all this in mind, we performed two new tests, one at 140 °C and a total pressure of 16 bar (8 bar partial pressure of carbon monoxide and 8 bar partial pressure of hydrogen), and a second one at 150 °C and a total pressure of 10 bar (again with a carbon monoxide to hydrogen ratio of 1); tests number 15 and 16 in Table 1.

Test 15 exhibited a conversion of 76.5% with 100% selectivity to hydroformylation products, and a SELB of 34.6% (the smallest selectivity obtained for the branched in this study, or 65.4% SELL), in good agreement with equation 9 (Figure 6), which predicted a mean selectivity of 36.8% and a confidence interval between 32.7 and 41.0% for an individual measurement (Figure S13). The parity plot also shows the good agreement between the predicted and actual values of selectivity obtained for experiment 15 (diamond symbol in Figure S13). Experiment 16, at 150 °C and 10 bar pressure, did not show conversion.

Comentat [A6]: Maybe you could add the boiling temperature of the solvent here

Comentat [A7]: Because of solvent evaporation? Maybe you can explicitly say it here.

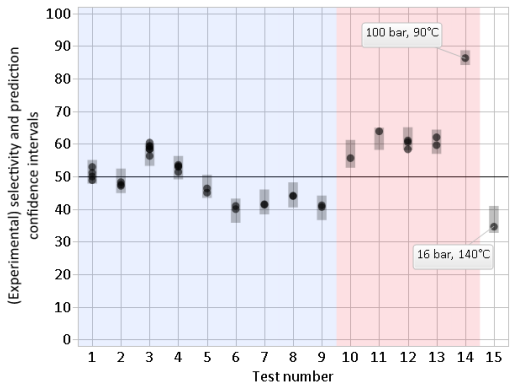

Figure 6. SELB (dots) and confidence intervals of the predictions using equation 9. Blue shadowed

are corresponds to the tests of the first experimental phase. Red shadowed area corresponds to the second experimental phase at higher pressures. White area corresponds to the test done at low pressure and high temperature to maximize SELL.

Our model predicts that at higher temperatures, a high carbon monoxide to hydrogen ratio while operating at a low hydrogen partial pressure is beneficial for the production of the linear product (Figure 7). Moreover, the model predicts a linear selectivity of 67% at 160 °C, however, the test was not conducted due to the consideration of the boiling point of toluene. We tried the test at 140 °C, 50 bar carbon monoxide and 5 bar hydrogen; however, despite the production of the linear hydroformylation product is favored over the branched product, we also observed the presence of the hydrogenated product, a competitive product to the hydroformylation reaction products. Our model is therefore not applicable as it was built under conditions where only hydroformylation products were obtained.

Comentat [A8]: One question for consideration here: how could you explain that hydrogenation products are favored when working at a CO/H2 ratio of 10? Whereas when working at a CO/H2 of 1 we only obtain hydroformylation products at the same temperature? This looks counter intuitive

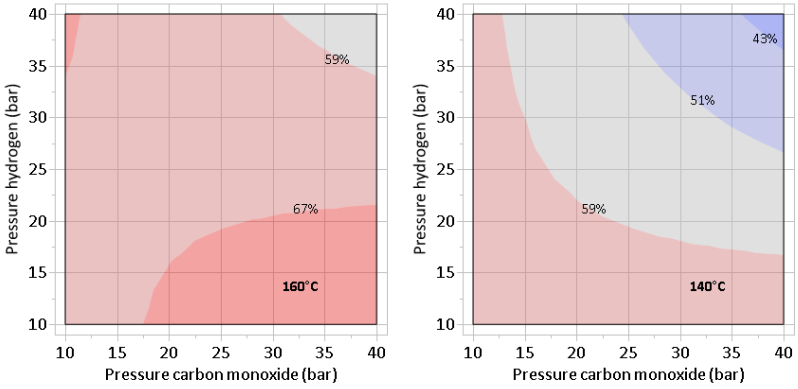

Figure 7. Contour plots for the selectivity towards the linear product with increasing temperature using Equation 9 as a function of the partial pressure of carbon monoxide and partial pressure of hydrogen.

Comentat [A9]: Maybe show the plot at 140°C first (to the left) and next the plot at 160°C (to the right)

Linear to branch ratio (l/b)

Switching from high selectivity to the branched product or to the linear product using the same catalyst and only changing the reaction conditions could represent a techno-economic advantage of using heterogeneous catalysts, and in particular of Rh/g-C_3N_4 catalysts in the hydroformylation of styrene. Using DOE, we have been able to produce models with as few as 9 tests (model 1) and 14 tests (model 2) that has led us to achieving a very high SELB of 86.3%, which represents a l/b of 0.16. According to our models, we could further increase the SELB by increasing the total pressure while working at a carbon monoxide to hydrogen ratio of 1; at a total pressure of 120 bar and 90 °C, we predict a SELB between 91.2% and 94.6%; increasing the pressure to 160 bar, the model predicts a SELB between 97.9% and 99.3%; and increasing the pressure to 200 bar, the model predicts a SELB between 99.6% and 100%.

Regarding the SELL, the best result we have obtained was 65.4% working at 140 °C and 16 bar total pressure, with a carbon monoxide to hydrogen ratio of 1. This represents a l/b of 1.89, a value slightly larger than the best result published by Axet and coworkers.[22] All further attempts to improve this result were deemed unsuccessful; in particular, a test at 150 °C and 10 bar total pressure did not show any conversion. Our model however predicts that increasing temperature and working at low partial pressure of hydrogen (i.e. 10 bar), but at a carbon monoxide to hydrogen ratio larger than 1 should favor the product of the linear product. Yet, our model also predicts a maximum SELL that seems to be a limit with the Rh/g-C_3N_4 catalyst. Figure 8 shows that at 140 °C, the model predicts that the highest mean SELL is slightly below 65%, and that this result can be obtained 20 bar total pressure with a carbon monoxide to hydrogen ratio of 1, or at higher pressures, but also increasing the carbon monoxide to hydrogen ratio. On the other hand, if we could work at 160 °C, the SELL could improve, although slightly up to about 70% at moderate pressure (i.e. 50 bar) and high carbon monoxide to hydrogen ratio (i.e. 4). According to the model, upon an increase in temperature to 180 °C and a drop in pressure to 2 bar, a linear selectivity of 75% would be expected. However, such variation could affect the chemoselectivity, which is not included in the

model.

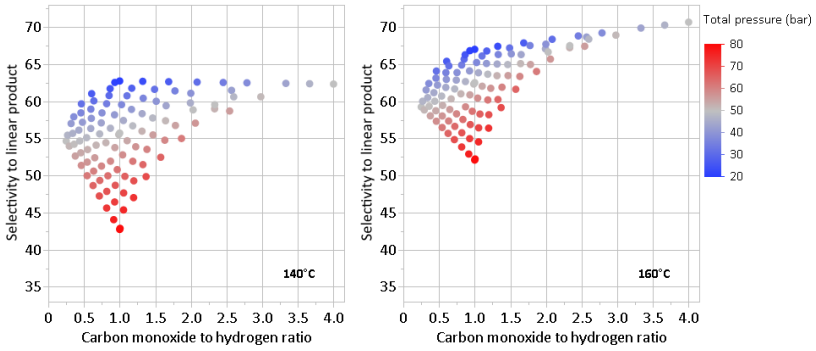

Figure 8. SELL as a function of the carbon monoxide to hydrogen ratio and total pressure. (left) predicted SELL at 140 °C, (right) predicted SELL at 160 °C.

CONCLUSIONS

A DOE method was employed to assess the impact of the reaction temperature, partial pressure of carbon monoxide and partial pressure of hydrogen on the hydroformylation of styrene over a highly dispersed Rh/g-C_3N_4 catalyst. No hydrogenated products were obtained in any tests indicating high hydroformylation selectivity. Regarding the regioselectivity, an empirical model for the prediciton of correlating SELB ~~with tested parameters~~as a function of the process parameters was developed and both the SELB and SELL were maximized~~optimized~~. Through this methodology, high regioselectivity towards either the branched or the linear aldehyde product could be achieved by adjusting the reaction conditions. Therefore, the results from this study could be applied for the selective production of these products. Lower temperatures and higher pressures favor the branched product with a selectivity of 86.3% at 90 °C and 100 bar total pressure of CO/H_2 (1:1) and predicting a 100 % SELB at 90 °C and 200 bar pressure of CO and H_2 in a 1:1 ratio. Conversely, higher temperatures and lower pressures promote the formation of the linear product,

Comentat [A10]: It is not correlated as we used design of experiments. I will explain you the difference another day.

which influenced by solvent properties and other variables.

ASSOCIATED CONTENT

Data Availability Statement

All data are provided in the manuscript and the Supporting Information.

Supporting Information

The Supporting Information is available free of charge at https: It includes all information on catalyst characterization, experimental results and the computational details.

AUTHOR INFORMATION

Corresponding Authors

Daniel Curulla-Ferré - *TotalEnergies OneTech Belgium, Feluy B7181, Belgium*; orcid.org/0000-0002-9001-7425; E-mail: daniel.curulla-ferre@totalenergies.com, daniel.curulla@urv.cat

Cyril GODARD - *Department de Química Física i Inorgànica, Universitat Rovira i Virgili, Tarragona 43007, Spain*; orcid.org/0000-0001-5762-4904; E-mail: cyril.godard@urv.cat

Authors

Jie Pan - *Departament de Química Física i Inorgànica, Universitat Rovira i Virgili, Tarragona 43007, Spain*; orcid.org/ orcid.org/0000-0002-9761-5938; E-mail: jie.pan1@fundacio.urv.cat

Sergi Plana Ruiz - *Servei de Recursos Científics i Tècnics, Universitat Rovira i Virgili, Tarragona 43007, Spain*; orcid.org/0000-0002-4047-8362; E-mail: sergi.plana@urv.cat

Mostafa Taoufik - *Univ. Lyon 1, CPE Lyon, CNRS UMR 5128, Laboratoire de Catalyse PolymérisationProcédés et Matériaux (CP2M), Université de Lyon, F-69616, Fran*ce; orcid.org/0000-0002-3627-5263; Email: mostafa.taoufik@univ-lyon1.fr

Josep M. Ricart - *Departament de Química Física i Inorgànica, Universitat Rovira i Virgili, Tarragona 43007, Spain*; orcid.org/0000-0002-2610-5535; E-mail: josep.ricart@urv.cat

Author Contributions

The manuscript was written through contributions of all authors. All authors have given approval to the final version of the manuscript. Jie Pan performed all experiments and calculations under the supervision of Daniel Curulla-Ferré, Cyril Godard and Josep M. Ricart. Sergi Plana-Ruiz and Mostafa Taoufik helped on the HAADF-STEM and CO adsorbed DRIFT, respectively.

Funding Sources

This work was supported by (PID2021-128128NB-I00 and PID2019-104427RB-I00) from MICIU/AEI/10.13039/501100011033 and "FEDER/UE", and (2021SGR00110 and 2021SGR00163) from Generalitat de Catalunya. Jie Pan is thankful to AGAUR (grant number 2020-FISDU-00174). The HRTEM was partially funded by the operative program FEDER Catalunya 2014-2020 (IU16-015844).

ACKNOWLEDGMENT

HAADF-STEM and CO adsorbed DRIFT were performed at the "Servei de Recursos Científics i Tècnics de la Universitat Rovira i Virgili" in Tarragona and Laboratory of Catalysis, Polymerization, Processes and Materials (CP2M) located at the CPE-Lyon engineering school on the campus of the DOUA in Villeurbanne, respectively. The authors thank Dr. Kai C. Szeto for his help when performing in CO adsorbed DRIFT measurement. The authors thank Dr. Maria D. Fernández-Martínez and Dr. Jèssica Margalef-Pallarès for their help in catalyst synthesis and testing.

REFERENCE

Comentat [A11]: Why are some references highlighted in yellow?

(1) Liu, A. Y.; Cohen, M. L. Prediction of New Low Compressibility Solids. *Science* **1989**, *245*, 841-842.

(2) Dong, G.; Zhang, Y.; Pan, Q.; Qiu, J. A fantastic graphitic carbon nitride (g-C_3N_4) material: Electronic structure, photocatalytic and photoelectronic properties. *J. Photochem. Photobiol. C* **2014**, *20*, 33-50.

(3) Patnaik, S.; Sahoo, D. P.; Parida, K. Recent advances in anion doped g-C_3N_4 photocatalysts: A review. *Carbon* **2021**, *172*, 682-711.

(4) Xiao, X.; Zhang, L.; Meng, H.; Jiang, B.; Fu, H. Single Metal Atom Decorated Carbon Nitride for Efficient Photocatalysis: Synthesis, Structure, and Applications. *Sol. RRL* **2021**, *5*, 2000609-2000629.

(5) Rocha, G. F. S. R; da Silva, M. A. R.; Rogolino, A.; Diab, G. A. A.; Noleto, L. F. G.; Antonietti, M.; Teixeira, I. F. *Chem. Soc. Rev.* **2023**, *52*, 4878-4932.

(6) a) Roelen, O. Pioneer in Industrial Homogeneous Catalysis. *Chem. Abstr.* **1994**, *38*, 550-554; b) Roelen, O. (Chemische Verwertungsgesellschaft, mBH Oberhausen), DE Patent 849-584, **1938/1952**; c) Roelen, O. US Patent 2 317 066 , **1943**.

(7) Wiese, K. D.; Obst, D. in *Catalytic Carbonylation Reactions* (Ed.: M. Beller) Springer, Berlin Heidelberg, **2010**, 1-33; b) Weissermel, K.; Arpe, H. J. in *Industrial Organic Chemistry*, Wiley-VCH Verlag GmbH **2008**, 127-144.

(8) Klosin, J.; Landis, C. R. Ligands for practical rhodium-catalyzed asymmetric hydroformylation. *Acc. Chem. Res*. **2007**, *40*, 1251-1259; b) Breit, B. Nickel-Catalyzed Reductive Couplings of Aldehydes and Alkynes. *Top. Curr. Chem.* **2007**, *279*, 139-172; c) Ungvári, F. Application of transition metals in hydroformylation: Annual survey covering the year 2006. *Coord. Chem. Rev*. **2007**, *251*, 2087-2102; d) Ungvári, F. Application of transition metals in hydroformylation: Annual survey covering the year 2005. *Coord. Chem. Rev*. **2007**, *251*, 2072-2086; e) Wiese, K. D.; Obst, D. Hydroformylation. *Top. Organomet. Chem*. **2006**, *18*, 1-33; f) Gual, A.; Godard, C.; Castillón, S.; Claver, C. Highlights of the Rh-catalysed asymmetric hydroformylation of alkenes using phosphorus donor ligands. *Tetrahedron: Asymmetry* **2010**, *21*, 1135-1146; g) van Leeuwen, P. W.

N. M.; Kamer, P. C. J.; Claver, C.; Pàmies, O.; Diéguez, M. Phosphite-containing ligands for asymmetric catalysis. *Chem. Rev.* **2011**, *111*, 2077-2118.

(9) Breit, B. Aldehydes: synthesis by hydroformylation of alkenes. in *Science of synthesis*, Brückner, R. **2007**, 277-317.

(10) Van Leeuwen, P. W. N. M. in *Homogeneous Catalysis: Understanding the Art*, Kluwer, Dordrecht **2004**, Chapter 8 and references therein.

(11) Sun, Q.; Jiang, M.; Shen, Z.; Jin, Y.; Pan, S.; Wang, L.; Meng, X.; Chen, W.; Ding, Y.; Li, J.; Xiao, F. S. Porous organic ligands (POLs) for synthesizing highly efficient heterogeneous catalysts. *Chem*. *Commun*. **2014**, *50*, 11844-11847.

(12) Sun, Q.; Dai, Z.; Liu, X.; Sheng, N.; Deng, F.; Meng, X.; Xiao, F. S. Highly Efficient Heterogeneous Hydroformylation over Rh-Metalated Porous Organic Polymers: Synergistic Effect of High Ligand Concentration and Flexible Framework. *J*. *Am*. *Chem*. *Soc*. **2015**, *137*, 5204-5209.

(13) Wu, X. F.; Fang, X.; Wu, L.; Jackstell, R.; Neumann, H.; Beller, M.; Transition-metal-catalyzed carbonylation reactions of olefins and alkynes: a personal account. *Acc*. *Chem*. *Res*. **2014**, *47*, 1041-1053.

(14) Lang, R.; Li, T.; Matsumura, D.; Miao, S.; Ren, Y.; Cui, Y. T.; Tan, Y.; Qiao, B.; Li, L.; Wang, A.; Wang, X.; Zhang, T. Hydroformylation of Olefins by a Rhodium Single-Atom Catalyst with Activity Comparable to $RhCl(PPh_3)_3$. *Angew. Chem. Int. Ed.* **2016**, *55*, 16054-16058.

(15) Amsler, J.; Sarma, B. B.; Agostini, G.; Prieto, G.; Plessow, P. N.; Studt, F. Prospects of Heterogeneous Hydroformylation with Supported Single Atom Catalysts. *J*. *Am*. *Chem*. *Soc*. **2020**, *142*, 5087-5096.

(16) Tang, P.; Paganelli, S.; Carraro, F.; Blanco, M.; Riccò, R.; Marega, C.; Badocco, D.; Pastore, P.; Doonan, C. J.; Agnoli, S. Postsynthetic Metalated MOFs as Atomically Dispersed Catalysts for Hydroformylation Reactions. *ACS Appl*. *Mater*. *Interfaces* **2020**, *12*, 54798-54805.

(17) Gong, H.; Zhao, X.; Qin, Y.; Xu, W.; Wei, X.; Peng, Q.; Ma, Y.; Dai, S.; An, P.; Hou, Z. Hydroformylation of olefins catalyzed by single-atom Co(II) sites in zirconium phosphate. *J*. *Catal*. **2022**, *408*, 245-260.

(18) Escobar-Bedia, F. J.; Lopez-Haro, M.; Calvino, J. J.; Martin-Diaconescu, V.; Simonelli, L.; Perez-Dieste, V.; Sabater, M. J.; Concepción, P.; Corma, A. Active and Regioselective Ru Single-Site Heterogeneous Catalysts for Alpha-Olefin Hydroformylation. *ACS Catal*. **2022**, *12*, 4182-4193.

(19) Zhao, K.; Wang, H.; Wang, X.; Li, T.; Dai, X.; Zhang, L.; Cui, X.; Shi, F. Confinement of atomically dispersed Rh catalysts within porous monophosphine polymers for regioselective hydroformylation of alkenes. *J*. *Catal*. **2021**, *401*, 321-330.

(20) Wei, B.; Liu, X.; Hua, K.; Deng, Y.; Wang, H.; Sun, Y. Effectively Regulating the Microenvironment of Atomically Dispersed Rh through Co and Pi to Promote the Selectivity in Olefin Hydroformylation. *ACS Appl*. *Mater*. *Interfaces* **2021**, *13*, 15113-15121.

(21) Chen, T.; Li, F.; Lang, R.; Wang, H.; Su, Y.; Qiao, B.; Wang, A.; Zhang, T. Hydroformylation of Styrene Derivatives Catalyzed by Rhodium Single-Atoms Supported on CeO_2. *Angew. Chem. Int. Ed.* **2020**, *59*, 7430-7434.

(22) Jurado, L.; Esvan, J.; Luque-Álvarez, L. A.; Bobadilla, L. F.; Odriozola, J. A.; Posada-Pérez, S.; Poater, A.; Comas-Vives, A.; Axet, M. R. Highly dispersed Rh single atoms over graphitic carbon nitride as a robust catalyst for the hydroformylation reaction. *Catal*. *Sci*. *Technol*. **2023**, *13*, 1425-1436.

(23) a) Carroll, F. I.; Melvin, M. S.; Nuckols, M. C.; Mascarella, S. W.; Navarro, H. A.; Thomas, J. B. N-Substituted 4β-Methyl-5-(3-hydroxyphenyl)-7α-amidomorphans Are Potent, Selective κ Opioid Receptor Antagonists. *J. Med. Chem.* **2006**, *49*, 1781-1791. b) Garner, P.; Kaniskan, H. U.; Hu, J.; Youngs, W. J.; Panzner, M. Asymmetric multicomponent (C+NC+CC) synthesis of highly functionalized pyrrolidines catalyzed by silver (I). *Org. Lett.* **2006**, *8*, 3647-3650. c) Jones, M. C.; Marsden, S. P.; Subtil, D. M. M. Efficient Asymmetric Synthesis of Quaternary (E)-Vinylglycines by Deconjugative Alkylation of Dehydroamino Acids. *Lett. Org.* **2006**, *8*, 5509-5512. d) Biddle, M. M.; Lin, M.; Scheidt, K. A. *J. Am. Chem. Soc.* **2007**, *129*, 3830-3831. e) Tennakoon, M. A.; Henninger, T. C.; Abbanat, D.; Foleno, B. D.; Hilliard, J. J.; Bush, K.; Macielag, M. J. Synthesis and antibacterial activity of C_6-carbazate ketolides. *Bioorg. Med. Chem. Lett.* **2006**, *16*, 6231-6235.

(24) Ritesh, J. D.; Subhra, M.; Virendra Kumar, G. Synthesis of Functionalized Styrene Butadiene

Rubber and Its Applications in SBR-Silica Composites for High Performance Tire Applications. *Ind. Eng. Chem. Res.* **2021**, *60*, 4517-4535.

(25) Ilaria, D.; Sanjib, B.; Sara, T.; Elisa., M.; Elisa, P.; Bruno, A. Styrene and substituted styrene grafted functional polyolefins via nitroxide mediated polymerization. *Polym. Chem.* **2018**, *9*, 307-314.

(26) Zhu, J.; Xiao, P.; Li, H.; Sonia, A. C. C. Graphitic Carbon Nitride: Synthesis, Properties, and Applications in Catalysis. *ACS Appl. Mater. Interfaces* **2014**, *6*, 16449-16465.

(27) Box, G. E. P.; Hunter, J. S.; Hunter, W. G. *Statistics for Experimenters: design, innovation and discovery*, 2nd edition, Wiley **2005**, 1-672.

(28) Goos, P.; Jones, B. *Optimal design of experiments: a case study approach*, 1st edition, Wiley **2011**, 1-304.

(29) Zheng, Y.; Lin, L.; Ye, X.; Guo, F.; Wang, X. Helical graphitic carbon nitrides with photocatalytic and optical activities. *Angew. Chem. Int. Ed.* **2014**, *53*, 11926-11930.

(30) Wu, M.; Yan, J. M.; Zhang, X. W.; Zhao, M. in *Applied Surface Science*, Elsevier B. V. **2015**, 196-200.

(31) Shcherban, N. D.; Mäki-Arvela, P.; Aho, A.; Sergiienko, S. A.; Yaremov, P. S.; Eränen, K.; Murzin, D. Y. Melamine-derived graphitic carbon nitride as a new effective metal-free catalyst for Knoevenagel condensation of benzaldehyde with ethylcyanoacetate. *Catal. Sci. Technol.* **2018**, *8*, 2928-2937.

(32) Dante, R. C.; Martín-Ramos, P.; Sánchez-Arévalo, F. M.; Huerta, L.; Bizarro, M.; Navas-Gracia, L. M.; Martín-Gil, J. Synthesis of crumpled nanosheets of polymeric carbon nitride from melamine cyanurate. *J. Solid State Chem.* **2013**, *201*, 153-163.

(33) Dante, R. C.; Sánchez-Arévalo, F. M.; Huerta, L.; Muñoz-Bisesti, F.; Marquez, D.; Martín-Ramos, P.; Lartundo-Rojas, L.; Chamorro-Posada, P.; Solorza-Feria, O. Photocatalytic activity of a new composite material of Fe (III) oxide nanoparticles wrapped by a matrix of polymeric carbon nitride and amorphous carbon. *Fullerenes Nanotubes and Carbon Nanostructures* **2017**, *25*, 630-636.

(34) Iqbal, W.; Dong, C.; Xing, M.; Tan, X.; Zhang, J. Eco-friendly one-pot synthesis of well-adorned mesoporous g-C_3N_4 with efficiently enhanced visible light photocatalytic activity *Catal. Sci. Technol.* **2017**, *7*, 1726-1734.

(35) Suter, T.; Brázdová, V.; McColl, K.; Miller, T. S.; Nagashima, H.; Salvadori, E.; Sella, A.; Howard, C. A.; Kay, C. W. M.; Corà, F.; McMillan, P. F. Synthesis, Structure and Electronic Properties of Graphitic Carbon Nitride Films. *J. Phys. Chem. C* **2018**, *122*, 25183-25194.

(36) Chebanenko, M. I.; Zakharova, N. V.; Lobinsky, A. A.; Popkov, V. I. Ultrasonic-Assisted Exfoliation of Graphitic Carbon Nitride and its Electrocatalytic Performance in Process of Ethanol Reforming. *Semiconductors* **2019**, *53*, 2072-2077.

(37) Liu, B.; Huang, N.; Wang, Y.; Lan, X.; Wang, T. Promotion of Inorganic Phosphorus on Rh Catalysts in Styrene Hydroformylation: Geometric and Electronic Effects. *ACS Catal.* **2021**, *11*, 1787-1796.

(38) Hoerl, R. W.; Snee, R. D. *Statistical Thinking: Improving business performance*, 3rd edition, Wiley **2020**, 1-55.

Graphical Abstract